International Geology Review

ISSN: (Print) (Online) Journal homepage: https://www.tandfonline.com/loi/tigr20

Tethyan oceans reconstructions with emphasis on the Early Carboniferous Pir-Eshagh A-type rhyolite and the Late Palaeozoic magmatism in Iran

Susan Jamei , Mansour Ghorbani , Ian S. Williams & Mohsen Moayyed

INTERNATIONAL GEOLOGY REVIEW
https://doi.org/10.1080/00206814.2020.1768443

Tethyan oceans reconstructions with emphasis on the Early Carboniferous Pir-Eshagh A-type rhyolite and the Late Palaeozoic magmatism in Iran

Susan Jamei[a,b], Mansour Ghorbani[a], Ian S. Williams[b] and Mohsen Moayyed[c]

[a]Faculty of Earth Sciences, Shahid Beheshti University, Tehran, Iran; [b]Research School of Earth Sciences, Australian National University, Canberra, Australia; [c]Department of Earth Sciences, Faculty of Natural Sciences, University of Tabriz, Tabriz, Iran

ABSTRACT

The Late Palaeozoic rock associations, in particular A-type igneous rocks, of Iran are rarely exposed, but they are key to reconstructing the evolutionary history of the Tethyan oceans. Zircon U–Pb dating of a representative rhyolite sample from Pir-Eshagh, NW Iran, yields an Early Carboniferous (Visean) crystallization age of 340 ± 2.7 Ma. The extrusive rhyolite has the chemical characteristics of the A_1 subtype of A-type magmas, providing evidence for a magmatic activity within extensional basin. The composition of rocks is metaluminous to slightly peraluminous and K-rich, with trace element signatures similar to those of OIB. Low Y/Nb and Ce/Nb ratios are consistent with a combination of source enrichment and crustal contamination and ultimately that the studied rhyolites have formed by fractional crystallization from an enriched mantle-derived mafic parental magma, with crustal interactions. Palaeogeographic reconstructions of the Tethyan oceans and their borders imply that the Proto-Tethys Ocean has not spread in Iranian plate, although evidence for Paleo-Tethys and Neo-Tethys in the form of ophiolitic units is well-preserved. The Late Palaeozoic magmatic rocks of Iran define a trend parallel to the ridge separating Neo-Tethys the Iranian plate from Arabia and demonstrate that the separation of the Cimmerian terranes from northern Gondwana by the opening of the Neo-Tethys Ocean, and their drift northwards, began in the Late Devonian to Early Carboniferous.

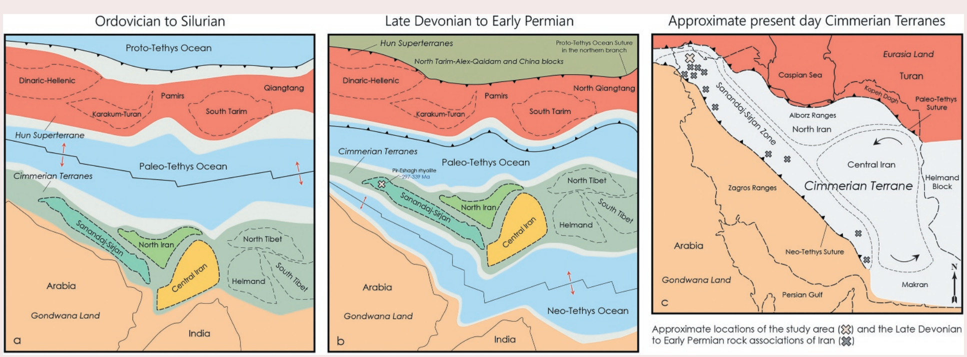

ARTICLE HISTORY

KEYWORDS
Proto-Tethys; -Paleo-Tethys; Neo-Tethys; Iran; -Pir-Eshagh rhyolite

1. Introduction

Stratigraphic and palaeomagnetic evidence indicates that Iran was connected to Gondwana from the Neoproterozoic until the Early Mesozoic, most likely as an extension of the Afro-Arabian continental platform. It became detached during the opening of the Neo-Tethys Ocean (Berberian and King 1981). The geological evolution of the Iranian plateau is related to the separation of continental segments from the northern Gondwana margin that then accreted to Eurasia during the Early Mesozoic (Berberian and King 1981; Stampfli 2000). Three successive ocean basins developed known as the Tethyan Oceans; Proto-Tethys, Paleo-Tethys and Neo-Tethys. Identifying the remnants of these basins, reconstructing their evolutionary history and the linkage between Gondwana and Eurasia in Iran have been long-debated issues. There is no consensus about the reconstruction of the Tethyan oceans, a key aspect of Iranian geology that remains poorly understood. The Palaeozoic period was accompanied by the development of Tethyan oceans and also Caledonian, Hercynian (or Variscan) and Cimmerian orogenic systems respectively. The Ordovician to Early Devonian Caledonian orogeny affected mostly the North Atlantic region. Closure of the Caledonian (Iapatus) Ocean

CONTACT Mansour Ghorbani m_ghorbani@hotmail.com; m-ghorbani@sbu.ac.ir Faculty of Earth Sciences, Shahid Beheshti University, Tehran, Iran
The supplemental data for this article can be accessed here.

separating Laurentia (North America) and Baltica (northern Europe) resulted in a mountain range forming in northwestern Europe, the Caledonian fold belt (e.g. Berberian and King 1981). Iran was far from this collision zone and experienced only epeirogenic movements (e.g. Aghanabati 2006). The Hercynian belt, a series of mountain ranges, developed during the Late Carboniferous to Permo-Triassic (Sengör 1989; Schulmann *et al*. 2014) as a result of the convergence between, and subsequent collision of, Laurasia and Gondwana. This process involved several small microplates and fragments of magmatic arcs (Ziegler *et al*. 1979; Dias and Ribeiro 1995; Weil *et al*. 2001; Abalos *et al*. 2002). Most European scientists call Hercynian orogeny to be the main trigger for orogenic movements in Europe which some like to apply for some Carboniferous magmatism. The effects of the Hercynian orogeny in Iran is either epeirogenic similar to the previous phase (e.g. Berberian and King 1981). On contrary to Caledonian and Hercynian orogenic systems, Cimmerian orogeny is recorded in Iran by some rock associations and elongated strips of ophiolite and mélange, as Paleo-Tethys remains, in northern and central Iran (Figure 1) (e.g. Karimpour *et al*. 2006; Aghanabati 2006; Zanchetta *et al*. 2013; Shafaii Moghadam *et al*. 2015a; Topuz *et al*. 2018). The Cimmerian orogen resulted from the collision and accretion of several Peri-Gondwanan blocks to the southern margin of Eurasia between the Late Triassic and Early Jurassic, following the closure of the Paleo-Tethys ocean (Zanchetta *et al*. 2013).

We present new U–Pb date for magmatic zircon from one rhyolite, and whole-rock geochemical data from the associated rhyolite suite, and discuss the implications of the data along with previously studied Late Palaeozoic magmatic rocks of Iran in the context of the early rifting of Neo-Tethys and separation of Central Iran from Gondwana. We further review the brief evolutionary history of the Tethyan oceans and propose a comprehensive tectonic evolutionary model for those oceans.

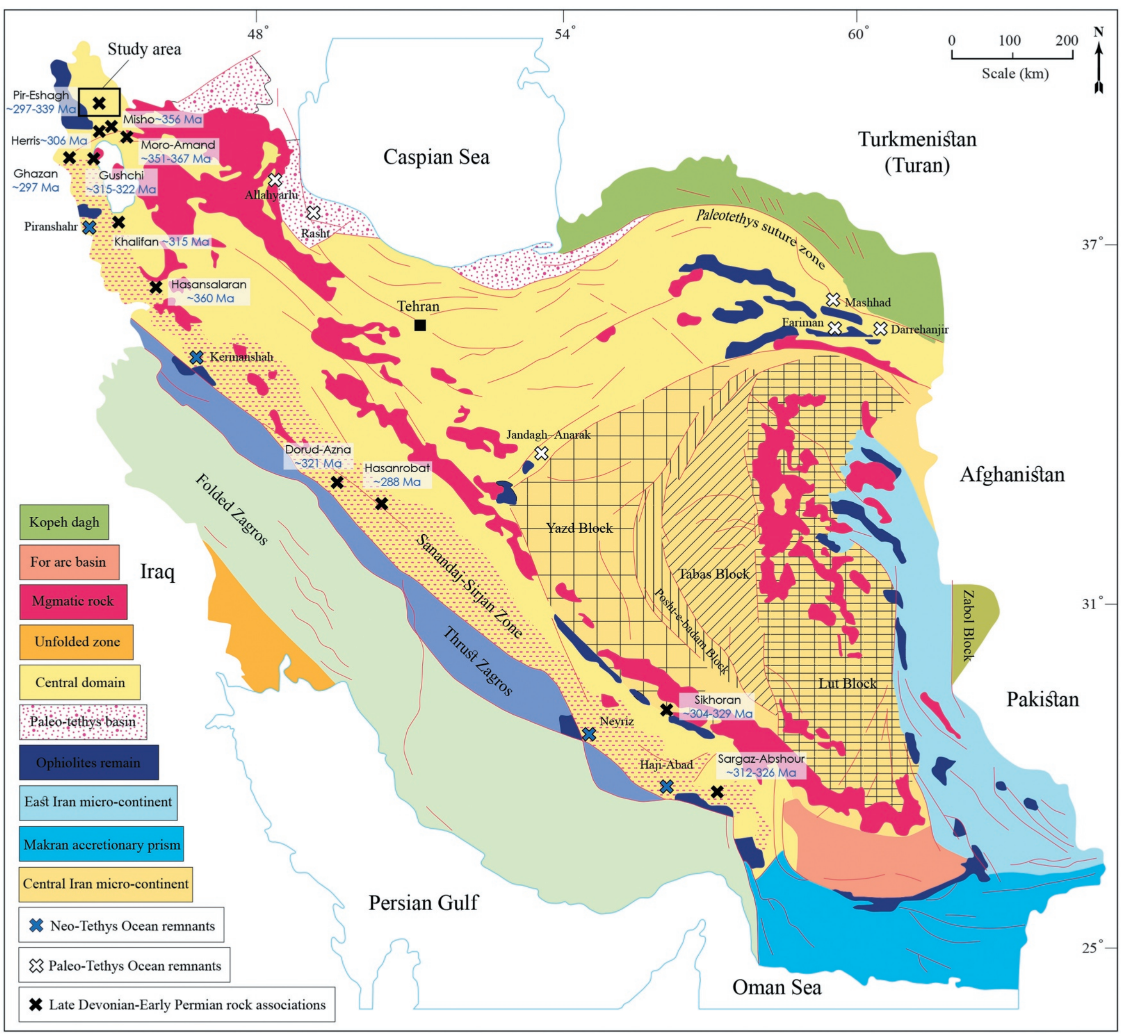

Figure 1. Major geological subdivisions of Iran after Nabavi (1976), with the location of the study area. Further information on the Late Devonian-Early Permian rocks is presented in Table 1.

Table 1. Late Palaeozoic rock associations from Iran.

Pluton	Suite	Type	Method	Age (Ma)	Error	Period	Tectonic setting	References
Hasanrobat	Granite	A (A1)	U-Pb	288.3	3.6	Early Permian	Within-plate Extensional	Alirezaei and Hassanzadeh 2012
	Granite	A (A1, A2)	U-Pb	294.2	2.5	Early Permian		Honarmand *et al.* 2017
Ghazan	Gabbro	-	U-Pb	297	6	Early Permian	Within-plate Extensional	Asadpour *et al.* 2013
Pir-Eshagh Ignimbrite rhyolite	A (A2)	U-Pb	297.8	4.4	Early Permian	Post-collisional Extensional	Delavari *et al.* 2019	
Herris	Granite	A	U-Pb	306	34	Late Carboniferous	Within-plate Extensional	Advay and Ghalamghash 2011
Ghushchi	Gabbronorite	A(A1, A2)	U-Pb	319.9	2.5	Late Carboniferous		Shafaii Moghadam *et al.* 2015b
	Gabbronorite	A (A1, A2)	U-Pb	316.8	2.3	Late Carboniferous		
	Granite	A (A1, A2)	U-Pb	318.4	2.3	Late Carboniferous		
	Granite	A (A1, A2)	U-Pb	317.3	1.9	Late Carboniferous		
	Granite	A (A1, A2)	U-Pb	322	2.9	Late Carboniferous		
Khalifan	Granite	A	U-Pb	315	2	Late Carboniferous	-	Bea *et al.* 2011
Dorud-Azna Metagabbro	-	U-Pb	314.6	3.7	Late Carboniferous	Within-plate Extensional	Shakerardakani *et al.* 2015	
Sargaz-Abshour Orthogneiss	-	U-Pb	312.2	4.1	Late Carboniferous	Extensional Regime	Shafaii Moghadam *et al.* 2017	
Sikhoran	Gneiss	-	K-Ar	304.9	7	Late Carboniferous	Within-plate Extensional	Ghasemi *et al.* 2002
Misho	Leucogabbro	-	U-Pb	356.7	3.4	Early Carboniferous	Within-plate Extensional	Saccani *et al.* 2013
Amand	Granite	A (A1,A2)	U-Pb	350.9	1.3	Early Carboniferous	Within-plate Extensional	Mohammadi *et al.* 2019
Dorud-Azna	Mafic Dike	-	Ar-Ar	321.3	0.55	Early Carboniferous	Within-plate Extensional	Shakerardakani *et al.* 2015
Sargaz-Abshour	Orthogneiss	-	U-Pb	318.7	4	Early Carboniferous	Extensional Regime	Shahzeidi *et al.* 2017
	Orthogneiss	-	U-Pb	326.3	3.3	Early Carboniferous		
Sikhoran	Granite	Anatectic	K-Ar	329.6	7.6	Early Carboniferous	Within-plate Extensional	Ghasemi *et al.* 2002
	Amphibolite	-	K-Ar	324.6	16.6	Early Carboniferous		
Pir-Eshagh Rhyolite	A (A1)	U-Pb	339.7	2.7	Early Carboniferous	Within-plate Extensional	Present study	
Hasansalaran	Granite	A (A1)	U-Pb	360.3	4.3	Late Devonian	Within-plate Extensional	Azizi *et al.* 2017
	Granite	A (A1)	U-Pb	360.7	5.6	Late Devonian		
Moro	Granite	A (A1, A2)	U-Pb	366.8	6.8	Late Devonian	Within-plate Extensional	Mohammadi *et al.* 2019

2. Geologic background

Iran consists of an assemblage of micro-continental blocks which separated from each other by fold-and-thrust belts formed during the opening and closing of the Tethyan oceanic basins (Stampfli 2000; Stampfli and Kozur 2006). According to Berberian and King (1981) Iran can be divided into three major structural units based on the ophiolite-bearing sutures: 1) the Zagros orogenic belt (southern unit); 2) the Central Iran unit; and 3) Kopeh-Dagh and Alborz belts (northern unit). These units have been further subdivided based on tectonic position, stratigraphy, nature of magmatic activity, metamorphism, structural style etc., (Figure 1).

The Zagros belt is located in southwest Iran. It forms the northern margin of the Arabian platform and preserves a record of the prolonged convergence between Eurasian and Arabia plates through Neo-Tethys, from subduction and obduction processes to present-day plate tectonic setting (Agard *et al*. 2011). The belt consists of a thick sedimentary sequence of Precambrian to Pliocene age (James and Wynd 1965) and it comprises two main structural units; the Zagros folded belt and the High Zagros or Zagros thrust zone (Figure 1). The High Zagros is bounded by two faults, the main Zagros reverse fault, and the main recent dextral fault; representing the Zagros (Neo-Tethys) suture zone between the Arabian and Eurasian plates with remnants of Neo-Tethys oceanic lithosphere (Berberian 1995; Bosold *et al*. 2005; Authemayou *et al*. 2006; Allen *et al*. 2013) (Figure 1).

The Central Iran unit, structurally one of the most complicated zones of Iran, was produced by multiple orogenic events (Ghorbani 2013). It consists of a Gondwana-derived terrane with a variety of geologic histories: Precambrian basement, Palaeozoic platform sediments, and Precambrian to Quaternary sedimentary and igneous rocks (e.g. Berberian and King 1981; Alavi 1991). It is disconnected from the Zagros fold and thrust belt by the Main Zagros Thrust and is bounded to the north and northeast by the Kopeh-Dagh and southern parts of the Caspian Sea (Figure 1). The Central Iran unit is assumed to represent an integral part of Gondwana during Precambrian, Infra-Cambrian, and possibly also Cambrian time that detached from Gondwana in the Palaeozoic (Soffel and Forster 1980) and finally reattached to the Gondwanan Afro–Arabian plate in the Early Cenozoic (Jafari *et al*. 2018 and reference therein). The Central Iran was stable during the Palaeozoic, but there were some epeirogenic tectonic movements in the Late Silurian to Early Devonian (Berberian and King 1981). The Central Iranian microplate is bounded by faults, fold-and-thrust belts and Late Cretaceous to Early Palaeocene ophiolite and ophiolitic melange (Shafaii Moghadam and Stern 2015).

The northern unit (Kopeh-Dagh and Alborz) is characterized by continental crust containing remnants of Paleo-Tethys oceanic lithosphere. The Kopeh-Dagh belt is an intra continental range and presents tectonic structures that are parallel to the Paleo-Tethys suture zone (Robert *et al*. 2014). This belt links with the adjacent Alborz belt by the western prolongation of the suture zone (Wilmsen *et al*. 2009). Therefore, the northern unit is distinguished from the central unit by the Late Palaeozoic suture zone in North Iran, which is at the northern foot of the Alborz Mountains in the south and the Kopeh-Dagh in the north. During the Early Jurassic, the Kopeh-Dagh and Turan was covered unconformably by coal-bearing continental clastic deposits, evidence that the Iranian and Turan (Eurasia) plates were united in the Late Triassic to Early Jurassic (Berberian and King 1981).

3. Field relations and petrography

The rhyolite body studied here, mapped as the Pir-Eshagh extrusion, is within the Central Iran domain (Figure 1). The study area, located south-west of the city of Jolfa in the East Azerbaijan province of NW Iran, consists mainly of abundant sedimentary and pyroclastic rocks with lesser amounts of metamorphic units (Figure 2). The igneous rocks are composed mainly of rhyolite, andesite-dacite (Carboniferous age) and associated pyroclastics including tuff and ignimbrite (Eocene age) (Figure 2). The dominance of sedimentation in the region started during the Devonian, and then a gap until Permian. A relatively short magmatic activity occurred in the Carboniferous. The Late Palaeozoic volcanic rocks comprise smaller and distinct units including slightly to highly weathered reddish-brown rhyolite and andesite dacite (not studied here) (Figures 2 and 3a). Rhyolites were intruded into sedimentary deposits with fossils of Late Devonian (Centrorhynchus letiensis; Gosselet 1879) (Figure 3b) and were unconformably overlain by Permian sequences, suggesting its Carboniferous age. This succession was subsequently dismembered during the Mesozoic and Cenozoic by latter faulting (Figure 3c). Rhyolitic rocks mostly display a porphyritic to glomeroporphyritic texture and in some cases spherulitic and amygdaloidal growths. They present approximately 40% of quartz, K-feldspar, and plagioclase phenocrysts immersed in a fine matrix. The groundmass is a mixture of quartz and K-feldspar generated mainly or entirely by devitrification of glass. Magnetite, apatite, and zircon are accessory minerals. There are no biotites or amphiboles in the rhyolites. Quartz phenocrysts are euhedral to subhedral, with corrosion gulfs. Plagioclase phenocrysts show partly resorbed rims and have been variably sericitized (Figure 3d). K-feldspar phenocrysts commonly show rectangular crystal shapes and occasionally are partially surrounded by

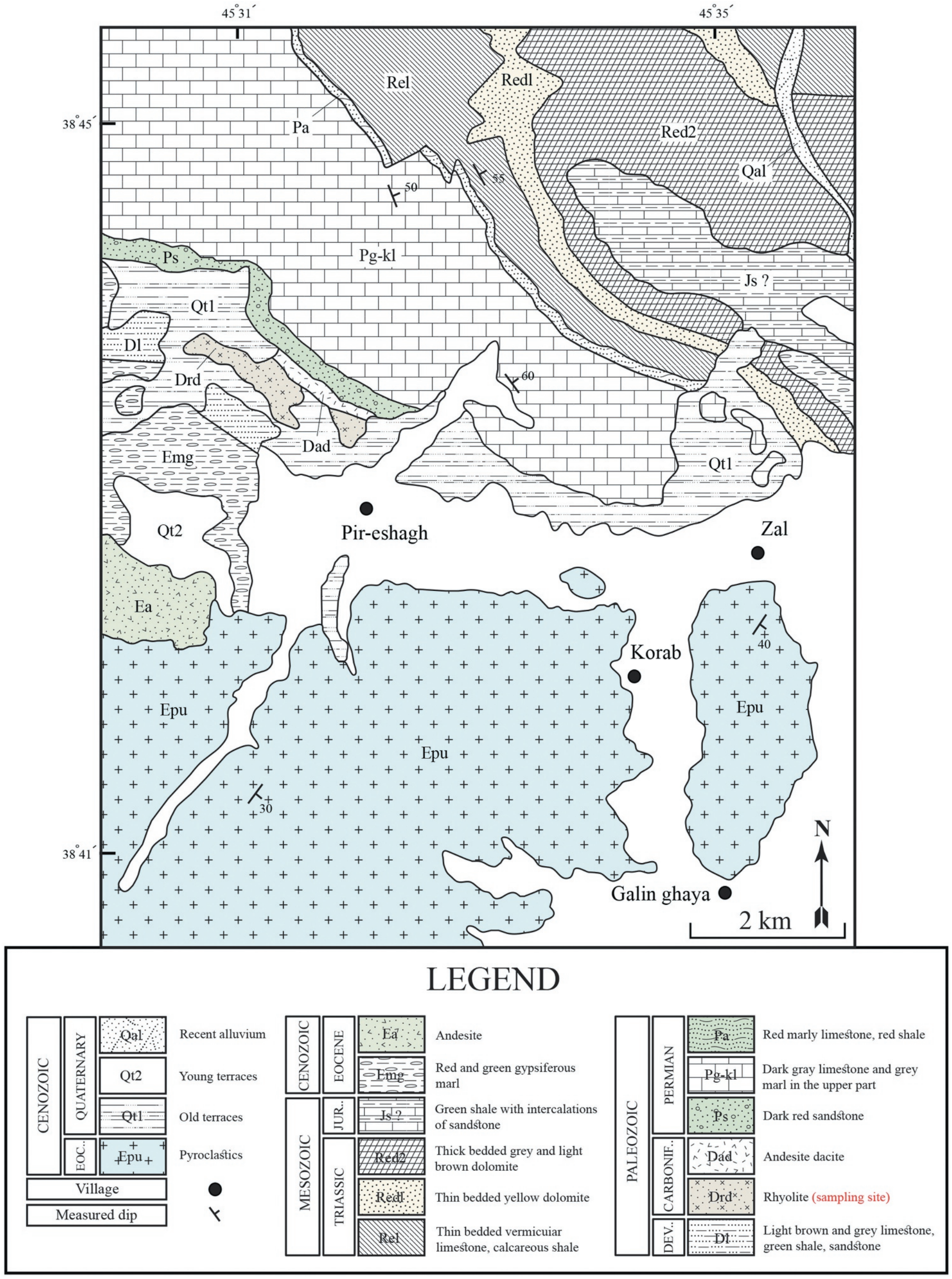

Figure 2. Sketch geological map of the study area.

plagioclase crystals (Figure 3e). Some microperthite is also present.

4. Analytical methods

4.1. Major and trace elements

Twenty samples of rhyolite were collected and checked for freshness using polished thin sections. Ten of the samples, with minimal petrographic evidence of late hydrothermal alteration, were selected for geochemistry. These were chipped by hand-splitter and powdered in a tungsten-carbide ring mill to a grain size of <200 mesh. Aliquots of each powder were sent to the ALS Brisbane laboratory, Australia, for whole rock analysis by geochemistry method ME-MS81d (ME-MS81 plus whole rock). Major oxide concentrations were done by Inductively Coupled Plasma-Atomic Emission (ICP-AES) and trace elements were carried out by Inductively Coupled Plasma Mass Spectrometry (ICP-MS). For this purpose, 0.2 g of sample powder is added to 1.5 g lithium metaborate ($LiBO_2$), mixed well and fused in a furnace at 1000°C. The resulting melt is then cooled and dissolved in 100 mL of 5% HNO_3 acid solution. This

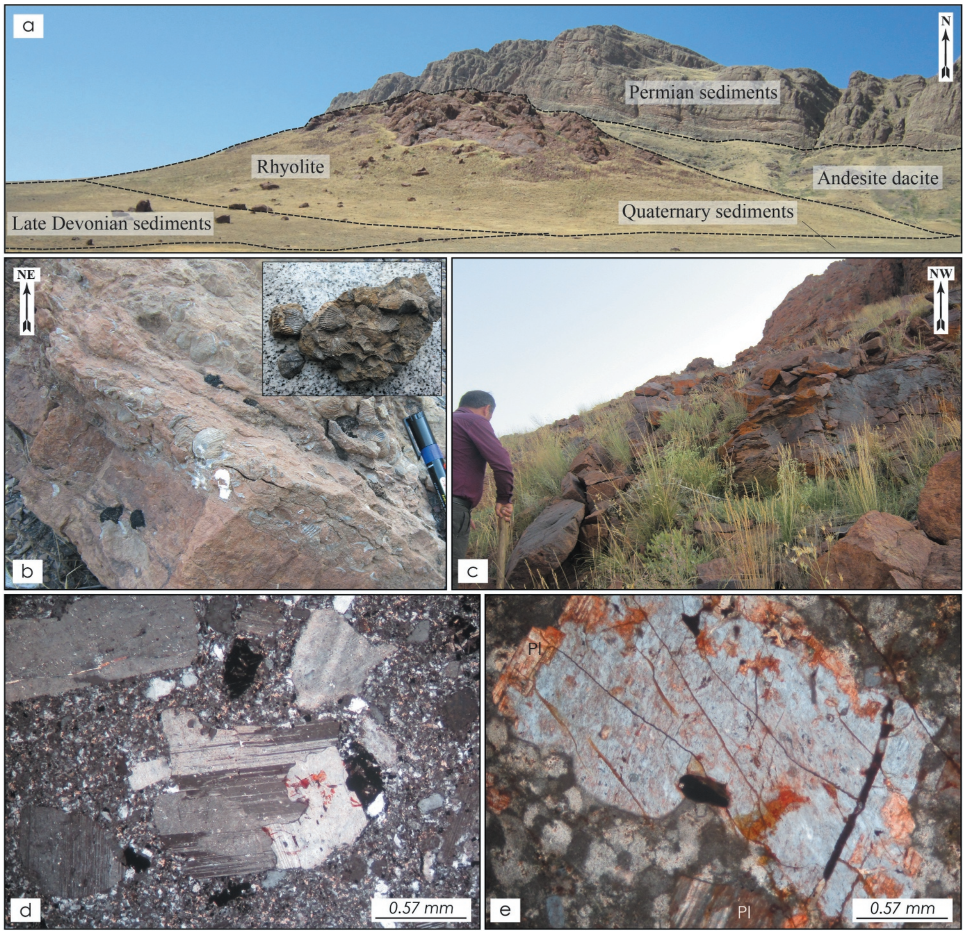

Figure 3. (a) Stratigraphic contact of the Pir-Eshagh rhyolite with Late Devonian and Permian sediments. (b) A sedimentary layer with fossils of Late Devonian (Centrorhynchus letiensis; Gosselet 1879). (c) Dismembered and weathered rhyolitic body. (d) Photomicrograph of a plagioclase phenocryst showing glomeroporphyritic texture in a fine-grained matrix. (e) Photomicrograph of a K-feldspar phenocrysts partially surrounded by plagioclase crystals.

solution is then analysed either by ICP-MS and ICP-AES. The accuracy of major elements is 0.01%, for most trace elements it is better than 10 ppm and for the rare earth elements (REE) it is 0.1 ppm or better. Results are reported in Supplementary file.

4.2. SHRIMP zircon U–Pb dating

Zircon U-Pb dating by SHRIMP (Sensitive High Resolution Ion Micro-Probe) is an accurate method for determining the crystallization ages of igneous rocks over a wide range of geological time. For the present work, separated zircon grains were dated using the SHRIMP-RG at the Research School of Earth Sciences (RSES), Australian National University (ANU), following the analytical procedure described by Williams (1998). U concentration was calibrated using reference zircon SL13 (238 ppm U, ~572 Ma) and Pb/U determined relative to reference zircon TEMORA 2 (417 Ma; Black *et al*. 2004). The radiogenic isotope ratios and calculated ages were corrected for common Pb using the measured ^{207}Pb, assuming concordance and a model common Pb composition consistent with the age of the grain (Gumming and Richards 1975) using Prawn and Lead software. All individual dates and weighted mean ages were calculated from the radiogenic ^{206}Pb/^{238} U. Data were plotted using Isoplot 3 (Ludwig 2003), showing the analyses before correction for common Pb. For all analyses the uncertainty in the determination of Pb/U and Pb/Th was set to a minimum of 0.5% to prevent the high precision analyses of high-U spots skewing the calculation of the weighted mean ages. The results are summarized in Supplementary file.

4.3. Electron microscope-cathodoluminescence (SEM-CL) imaging

Prior to SHRIMP analysis the sectioned, polished zircon crystals were imaged by cathodoluminescence (CL) using a JSM-6610A SEM at RSES, ANU, to reveal their morphology,

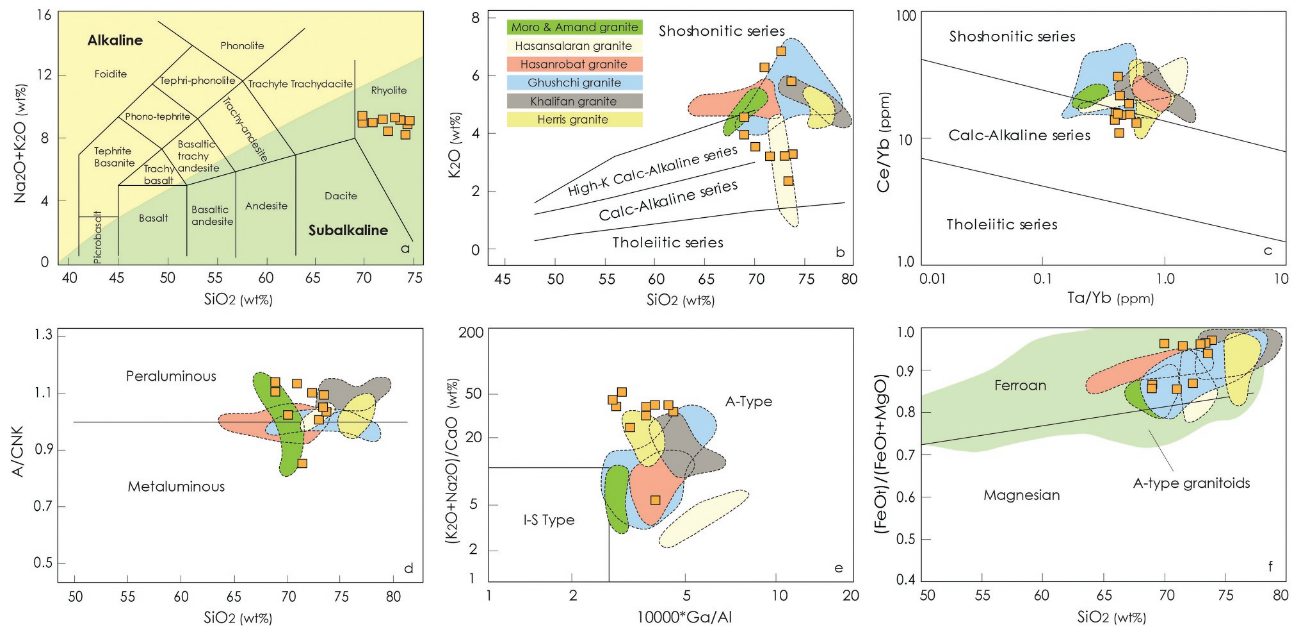

Figure 4. (a) Alkali-Silica diagram (TAS) for the chemical classification of volcanic rocks (Le Bas *et al.* 1986). The subalkaline-alkaline field boundary on the diagram is from Irvine and Baragar (1971). (b) SiO_2 vs. K_2O diagram (after Peccerillo and Taylor 1976). (c) Ta/Yb vs. Ce/Yb diagram (Pearce 1983). (d) SiO_2 vs. A/CNK diagram (Chappell and White 1974). (e) $(K_2O+Na_2O)/CaO$ vs. 10,000*Ga/Al diagram of Whalen *et al.* (1987). (f) SiO_2 vs. $FeO_t/(FeO_t+MgO)$ diagram of Frost *et al.* (2001) showing the affinity between the Pir-Eshagh rhyolite and A-type and ferroan rocks. Note that there are similar geochemical features between Pir-Eshagh rhyolite and the Late Palaeozoic A-type granites from Iran.

internal textures and paragenesis. These images were used in conjunction with transmitted and reflected light photomicrographs to determine the placement of the SHRIMP analytical spots, avoiding imperfections such as inclusions or fractures. In preparation for SEM imaging the epoxy grain mount was cleaned with petroleum spirit and warm RBS detergent solution, thoroughly rinsed in Millipore deionized water, and dried in a vacuum oven at 60°C for about one hour. The mount was then coated with ~2 nm of gold. This cleaning procedure was repeated prior to SHRIMP analysis, but the mount was dried for longer (overnight stay) and coated with a thicker layer of gold (~15 nm).

5. Results

5.1. Whole-rock geochemistry

Representative chemical analyses of the Pir-Eshagh rhyolite are listed in Supplementary file. The rock samples studied have a relatively narrow range of compositions, with high contents of SiO_2 (69.0–73.7 wt.%) and Na_2O+K_2O (8.18–9.16 wt.%), moderate contents of Al_2O_3 (12.80–14.70 wt.%), and low contents of TiO_2 (0.30–-0.56 wt.%), Fe_2O_3 t (2.44–4.49 wt.%), CaO (0.20–1.70 wt.%) and MgO (0.01–0.73 wt.%), consistent with their felsic mineralogy. Plotted on a total alkalis versus SiO_2 diagram (Lebas *et al.* 1986; Irvine and Baragar 1971), the rocks fall within the subalkaline rhyolite field (Figure 4a). Based on the biaxial diagram of K_2O vs. SiO_2 (Peccerillo and Taylor 1976) and Ta/Yb vs. Ce/Yb (Pearce 1983), they range from calc-alkaline to weakly shoshonitic (Figure 4b,c), with K_2O contents ranging from 2.33 to 6.82 wt.%, indicating their potassium-rich nature. All but one of the samples are peraluminous, with A/CNK (molecular Al_2O_3 $/(CaO+Na_2O+K_2O)$) of 1.14–0.85 (Figure 4d). All have high Ga/Al, plotting in the A-type field in the K_2O+Na_2O/CaO vs. Ga/Al diagram of Whalen *et al.* (1987) (Figure 4e). The rocks are ferroan according to the classification scheme of Frost *et al.* (2001), having $FeO_t/(FeO_t+MgO)$ ratios of0.84–0.99 (Figure 4 f). On the tectonic discrimination diagram of Pearce *et al.* (1984) based on the trace elements Rb, Y and Nb the samples fall tightly in the within-plate magmas (Figure 5a). The same is indicated by the Zr vs. Y diagram of Muller and Groves (1994) (Figure 5b). The primitive mantle normalized REE (McDonough and Sun 1995) and N-MORB normalized trace element abundance (Sun and McDonough 1989) patterns of all samples are very similar (Figure 6). The rocks are enriched in total REE (195–447 ppm), and particularly the light REE (Figure 6a), with high La_N/Yb_N (4.08–9.53), a pronounced negative Eu-anomaly (Eu/Eu* = 0.44–0.52) and relatively flat and undifferentiated heavy REE (Gd_N/Yb_N = 0.91–1.82). The high La_N/Sm_N (2.55–4.11) is consistent with fractionation of the LREE. Considering the multi-element variation diagram (Figure 6b), the rocks are enriched in the most incompatible

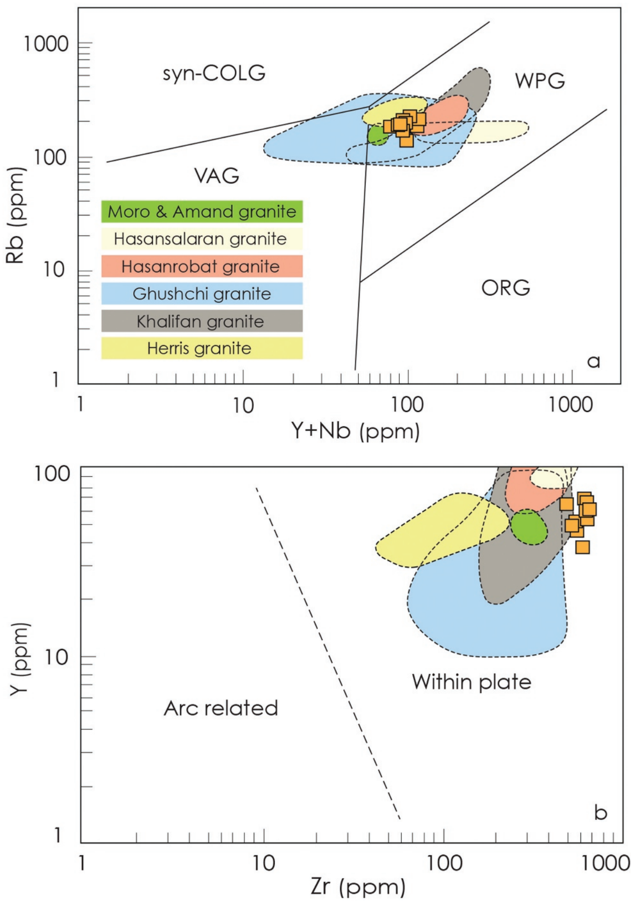

Figure 5. (a) Rb vs. Y+ Nb discrimination diagram of Pearce *et al.* (1984), and (b) diagram of Zr vs. Y (Muller and Groves 1994) showing a within-plate setting for the studied rhyolites. The Late Palaeozoic A-type granites from Iran also plot in the same fields.

elements and large ion lithophile elements (LILE: e.g. Rb, Ba, Th, La, U, and Ce) and depleted in Cs, Nb, Sr, P and Ti.

5.2. SHRIMP zircon U–Pb dating

Following the detailed petrography, sample P4was selected for zircon U-Pb dating. The zircon grains are relatively similar in size, shape and zoning textures (Figure 7), consistent with all having crystallized from the rhyolitic magma. They are euhedral to subhedral and relatively elongate, colourless, transparent, and without mineral inclusions. They have simple igneous banding with no visible or CL evidence for the presence of older cores. Their maximum size is about 300 μm. The 19 analyses of individual zircon grains define a single population within analytical uncertainty, with a weighted mean radiogenic $^{206}Pb/^{238}U$ age of 339.7 ± 2.7 Ma (95% c.l., MSWD = 1.5). Common Pb corrections were small, as evidenced by the near concordance of the uncorrected compositions (Figure 7). The U (54–199 ppm) and Th (21–113ppm) contents of the zircon are low. The Th/U ratios range from 0.38 to 0.92, typical of the range for igneous zircon crystallized from a felsic magma.

6. Discussion

6.1. Petrogenesis

The Pir-Eshagh rhyolite has chemical features, such as negative Sr, P, Ti and Eu anomalies, that are similar to those of A-type granitoids formed in within-plate settings (Whalen *et al.* 1996). A-type granitoids have been further divided into two subgroups of A_1 and A_2 on the basis of trace element abundances, particularly Y/Nb (Eby 1990, 1992). Group A_1, with Y/Nb ratios less than 1.2, includes rocks that have chemical characteristics similar to those of ocean-island basalts (OIB) and are thus mantle-derived, particularly in an intraplate or extensional tectonic regime. In contrast, the rocks of group A_2, with Y/Nb higher than 1.2, have an arc signature and are similar to rocks of continental crust or island arc basalts (IAB) formed at convergent plate margins, particularly in collisional and post-collisional settings (Eby 1992).

The Late Palaeozoic rock associations of Iran, especially in northwestern part, are distributed predominantly as mafic and felsic units like rhyolites of the present study and Ajabshir (Moayyed 2013), Misho granite and Ilanlu basalt (Jamei, unpublished data), Ghushchi gabbronorite and granite (Shafaii Moghadam *et al.* 2015b), Misho gabbro (Saccani *et al.* 2013) (comprehensive data in Table 1, Figure 1). This feature is interpreted to characterize the geotectonic setting of a bimodal suite in a non-orogenic environment. Enrichment in the LILE and LREE is indicative of within-plate rifting and continental break-up. The most likely process for the generation of the rhyolite is lithospheric extension, thinning of the lithosphere and upwelling of the asthenosphere to form a within-plate potassic magma. Such magmas are commonly characterized by OIB and MORB (mid-ocean ridge basalt) chemical affinities (Li *et al.* 2000; Gorring *et al.* 2003). In the Y/Nb vs. Rb/Nb and Y/Nb vs. Ce/Nb diagrams (Eby 1992), they plot mainly in the A_1 subgroup (Figure 8a,b). Furthermore, Figure 8b shows that the rhyolites fall within or near the OIB field, suggesting a source for the rhyolites similar to that of OIB, consistent with an intraplate setting (Figure 5). Detailed geochemical characteristics, however, show features of the A_2 subgroup (Y/Nb ratios in the range 0.86–1.65). This might be due to a range of oxygen fugacity as higher oxygen fugacity, by increasing Y/Nb, could push the samples to plot in the field of A_2 granitoids. The studied samples have $FeO_t/(FeO_t+MgO)$ ratios

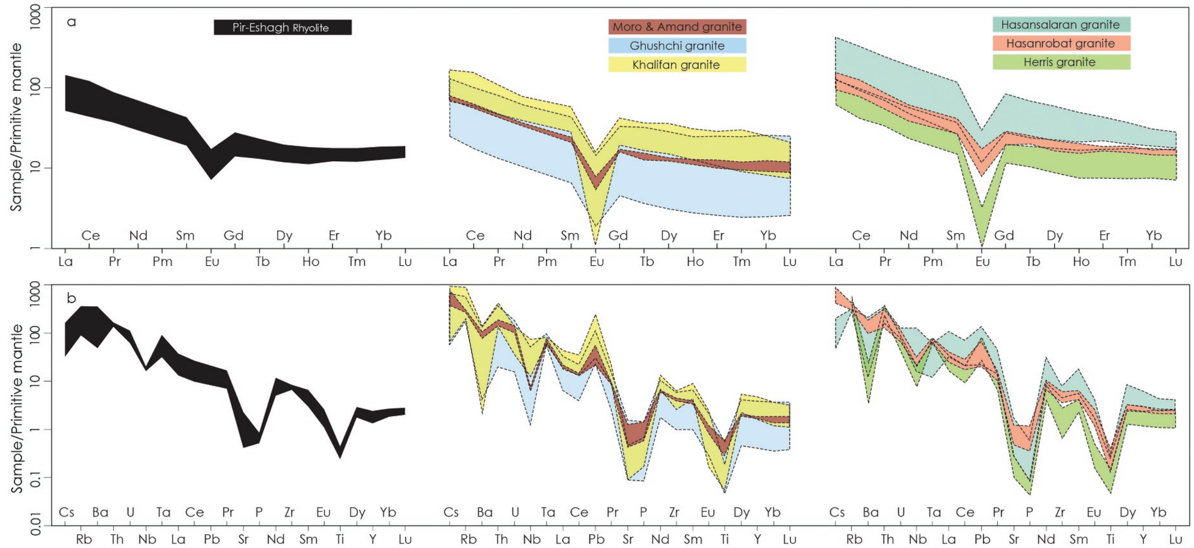

Figure 6. Normalized trace element diagrams for the Pir-Eshagh rhyolite and comparison with the Late Palaeozoic A-type granites form Iran. (a) Primitive mantle normalized REE compositions and (b) N-MORB-normalized multi-element patterns for the Pir-Eshagh rhyolite. Normalizing values are from McDonough and Sun (1995) and Sun and McDonough (1989) for (a) and (b) respectively. Note that trace element variations in the Late Palaeozoic A-type units of Iran are very similar, indicating probable same mechanism for their generation.

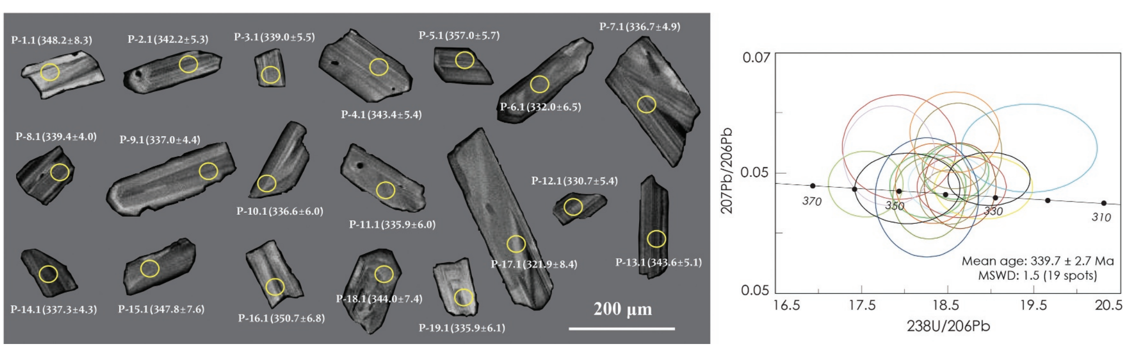

Figure 7. Representative Cathodoluminescence (CL) images showing internal structures of zircon grains form sample P4 and U–Pb Concordia diagram for the zircon analysed by ion microprobe.

of 0.86–0.99, which indicate that the rocks crystallized under a range of high to low oxygen fugacity conditions (Figure 8 c). Different oxygen fugacity conditions range from reduced to oxidized relevant to magma migration and emplacement (Kolzenburg *et al*. 2018). It is possible that the processes involved in the production of the rhyolites might have included some crustal contamination, given the low high Rb, Th, K, La and Cs observed in the samples (Figure 8d).

The petrogenesis of A-type granitoids remains controversial, and diverse scenarios have been proposed to explain the origin of these rocks: (1) extreme fractional crystallization of parental mafic magmas derived from the mantle, with or without crustal interactions (Loiselle and Wones 1979; Vander-Auwera *et al*. 2003), (2) high temperature partial melting of crustal rocks from which granitic magma has previously been extracted (Clemens *et al*. 1986; King *et al*. 1997), (3) partial melting of felsic granulites (Collins *et al*. 1982; Whalen *et al*. 1987), (4) partial melting of lower crustal anhydrous charnockite (Landenberger and Collins 1996), (5) partial melting of meta-igneous rocks (Creaser *et al*. 1991), (6) a metasomatic origin (Martin 2006) and (7) the combination of oceanic island basalts and crustal materials (Eby 1990, 1992). In addition, the rhyolitic magmas could be derived from various source materials, including enriched mantle, depleted mantle and felsic crust (Mbowou *et al*. 2015). Trace element ratios such as Nb/Ta and Zr/Hf are an effective means of recognizing the sources of volcanic rocks. The Nb/Ta (13.2–14.6) and Zr/Hf (38.0–41.1) ratios of the studied rhyolites are similar to those of OIB (Nb/Ta = 14.6–17.6; Zr/Hf = 35.5–45.5), while the estimated Nb/Ta ratio of the continental crust and the bulk-silicate Earth is ~12–13 and ~14, respectively

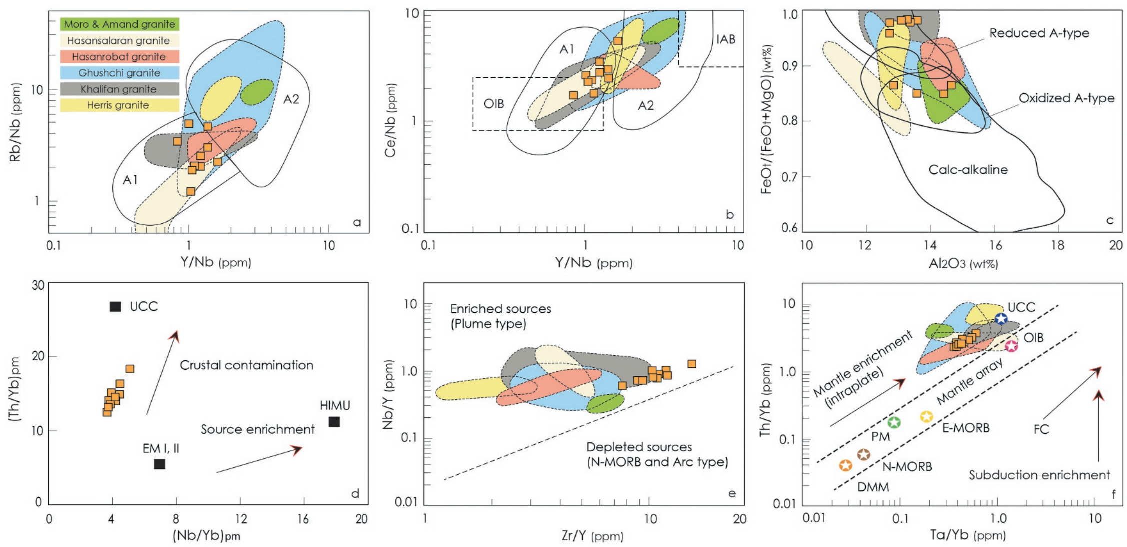

Figure 8. (a) Y/Nb vs. Rb/Nb, and (b) Y/Nb vs. Ce/Nb diagrams for the Pir-Eshagh A-type rhyolite (Eby 1992). Oceanic island basalt (OIB) and island arc basalt (IAB) fields are from Eby (1990). (c) $FeO_t/(FeO_t+MgO)$ vs. Al_2O_3 diagram showing the compositional fields of reduced and oxidized A-type rocks plus calc-alkaline granitoids (Dall'Agnol and de Oliveira 2007). (d) $(Th/Yb)_{pm}$ vs. $(Nb/Yb)_{pm}$ plot showing the crustal contamination trend for the Pir-Eshagh rhyolites. The ratios are normalized to primitive mantle values of McDonough and Sun (1995). Upper continental crust (UCC) composition is from Taylor and McLennan (1985), high U/Pb mantle source (HIMU) and enriched mantle sources (EM I and EM II) are from Condie (1997). (e) Nb/Y vs. Zr/Y diagram (Fitton *et al.* 1997). (f) Ta/Yb vs. Th/Yb diagram after Pearce (1983). All samples trend towards an enriched mantle source. Normal mid-ocean ridge basalt (N-MORB), enriched mid-ocean ridge basalt (E-MORB), primitive mantle (PM), and Ocean Island Basalt (OIB) depleted MORB mantle (DMM) compositions are from Sun and McDonough (1989). Upper continental crust (UCC) composition is from Taylor and McLennan (1985). Mantle array, subduction enrichment, and FC (fractional crystallization) approximate directions are from Pearce (1983). The Late Palaeozoic A-type granites from Iran are also compared to Pir-Eshagh rhyolite.

(Pfänder *et al.* 2007). A plot of Zr/Y vs. Nb/Y is useful in distinguishing between magmas derived from enriched (OIB or E-MORB) or depleted (N-MORB and subduction-related) sources (Fitton *et al.* 1997). All the rhyolite samples fall within the field of magmas derived from enriched sources (Figure 8e). Enrichment of the source is further indicated by the plot of Ta/Yb vs. Th/Yb (Pearce 1983) (Figure 8 f). In that plot, the rhyolites define a trend sub-parallel to, and above, the mantle enrichment array, consistent with the presence of crustal components. The elevated Th/Yb values could be due to the addition of a subduction component to mantle-derived magma, the melting of mantle contaminated by an earlier subduction process, or contamination of the magmas by continental crust (Raimo Lahtinen *et al.* 2016).

The compositions of rhyolitic magmas are controlled by a combination of source enrichment and possible crustal contamination, in the present case producing chemical signatures similar to those found in OIBs. This is consistent with the first scenario above – evolution; indicating that the study rhyolites have formed by fractional crystallization of an enriched mantle-derived parental mafic magma, with crustal interactions. The negative Eu anomalies are indicative of feldspar contention during fractionation and or partial melting process (Rollinson 1993). The negative Eu and Sr anomalies and unfractionated HREE suggest the presence of plagioclase and absence of garnet in the magma source (Rapp and Watson 1995; Nagudi *et al.* 2003) and the negative P and Ti anomalies can be attributed to residual apatite and ilmenite, respectively, in the source (Peng *et al.* 2012). The unfractionated HREE patterns and negative Eu and Sr anomalies could indicate that the magmas were produced under low pressure conditions (<1 GPa) where plagioclase is stable (Nagudi *et al.* 2003). At low pressures, plagioclase has a high affinity for Sr, while Y is more incompatible (Deng *et al.* 2018). Thus, Sr/Y ratios might possibly indicate the mean pressure or depth at which the magmas were generated. The studied rhyolites have relatively low Sr (<208 ppm) and high Y (37.7–67.6 ppm), hence low Sr/Y ratios (0.64–5.52) accompanied by negative Eu anomalies suggesting that plagioclase is residual in the source, and garnet is absent, implying that the magma was generated at low levels of pressure.

6.2. Geodynamic implications of Tethyan oceans

A review of the evolutionary history of the Tethyan oceans reveals that the Iranian micro-continents were far distant from the Proto-Tethys Ocean. Some researchers have argued, however, that there is geological evidence for the Proto-Tethys Ocean in Iran. For instance, the Takab Metamorphic Complex in NW Iran, with an age of ~560 Ma, has been interpreted as lithospheric remnants of Proto-Tethys (Hajialioghli *et al*. 2007; Saki 2010) and the Late Neoproterozoic-Cambrian granitoids in Iran, with ages ranging from 513 to 608 Ma, are generally attributed to the subduction of Proto-Tethys oceanic lithosphere beneath the Sanandaj-Sirjan and Central Iran (Shahzeidi *et al*. 2017; Badr *et al*. 2018). It is generally agreed that Proto-Tethys was an ancient, universal ocean basin that opened due to the break-up of the supercontinent of Rodinia in the Neoproterozoic (~600–580 Ma), evolved following initiation of subduction in the Cambrian (~520 Ma), and closed at the end of the Early Palaeozoic during the final assembly of Gondwana (e.g. von Raumer and Stampfli 2008; Zhang *et al*. 2012; Li *et al*. 2018; Zhao *et al*. 2018; Song *et al*. 2018). In Asia, the Proto-Tethys Ocean separated a collection of subcontinents to the north from the margin of Gondwana to the south bounded by the Hun (or Hunic) superterrane (von Raumer and Stampfli 2008; Zhao *et al*. 2018)(Figure 9). The northern block collided with Gondwana following south-dipping subduction during the Ordovician to Early Devonian (Stampfli and Borel 2002; von Raumer *et al*. 2013; Shumei *et al*. 2015; Li *et al*. 2018; Zhao *et al*. 2018), synchronous with the Caledonian orogeny. Accordingly, considering Proto-Tethys ocean lifetime (~600 to ~397 Ma) and its geographic location it could be argued that some geological evidence attributed to the Proto-Tethys Ocean in Iran were associated with an ocean that was the precursor of Proto-Tethys. The subduction of the Proto-Tethys oceanic plate beneath Gondwana coincided with the opening of the Paleo-Tethys Ocean in a back-arc extensional setting within the continental lithosphere along the trailing edge of the Hun Superterrane (Figure 9). This opening separated the Hun Superterrane from a series of Gondwanan terranes that formed the Cimmerian continent, which includes Central Iran (Stampfli 2000; Stampfli and Borel 2002; Torsvik and Cocks 2004). When the Paleo-Tethys Ocean opened is still a matter of debate. Torsvik and Cocks (2004) suggested that different independent microplates may indicate diachronous separation, and therefore that Paleo-Tethys opened at different times in different places. Mohammadi *et al*. (2019) have controversially interpreted that Amand and Moro A-type plutons, located in NW Iran, were generated as the result of Paleo-Tethys opening during Late Devonian-Early Carboniferous. It is widely accepted, however, that the opening occurred in the Ordovician to Silurian (e.g. Ziegler *et al*. 2001; Stampfli *et al*. 2001; Stampfli and Borel 2002; von Raumer *et al*. 2003; Li *et al*. 2018) and that the oceanic lithosphere developed mainly in the Carboniferous to Permian. The presence of Late Ordovician–Silurian rift-related flood basalts in northern Iran (Bagheri and Stampfli 2008) confirms that

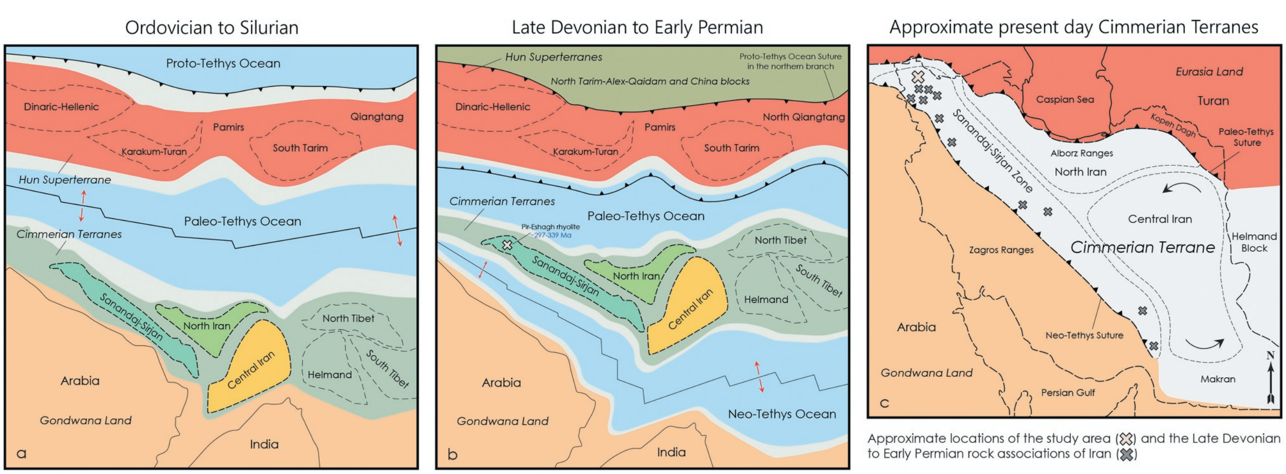

Figure 9. Palaeogeographic reconstruction of the Iranian Cimmerian micro-continents and their relationship to the Tethyan oceans. (a) Ordovician to Silurian reconstruction showing the southward subduction of the Proto-Tethys oceanic plate underneath the Hun Superterrane and its movement towards closing. It was coupled with the opening of Paleo-Tethys by rifting between the Hun Superterrane and Gondwana (Cimmerian Terranes). (b) Late Devonian to Early Permian plate-tectonic reconstruction showing Proto-Tethys closing and subsequent continental collision between the northern blocks and the Hun Superterrane. The Paleo-Tethys Ocean started northward subduction underneath the Hun Superterrane and the Cimmerian Terranes rifted away from Gondwana to form Neo-Tethys. (c) Approximate current tectonic setting of the Cimmerian micro-continent in Iran. Note that Central Iran has rotated 135° anticlockwise since the Triassic. (a) and (b) modified after Stampfli *et al*. (2001). Find out more information about the Late Devonian to Early Permian rock associations of Iran in Figure 1 and Table 1

Paleo-Tethys opened during that time. Well-preserved Late Devonian–Carboniferous magmatic arc products and the Triassic fore-arc succession (Bagheri and Stampfli 2008) and Late Palaeozoic magmatic arcs within the Turan Plate (Garzanti and Sciunnach 1997) reveal that the Paleo-Tethys subduction initiated beneath the Turan block (Eurasia) before 380 Ma (Late Devonian) (Shafaii Moghadam and Stern 2014). The final closure of the Paleo-Tethys Ocean and docking of the Iranian block to Eurasia took place during the Eo-Cimmerian orogenic cycle in the Late Triassic following northward subduction of the oceanic plate underneath Eurasia (Stampfli *et al*. 2001; Stampfli and Borel 2002; Liu *et al*. 2006; Bagheri and Stampfli 2008). The Early Jurassic coal-bearing continental clastic deposits to the north (Kopeh-Dagh and Turan) and south (Central Iran and Alborz) of the collisional zone indicate a united Iran-Turanplate in the Late Triassic to Early Jurassic and the end of the Paleo-Tethys Ocean (Berberian and King 1981). This timing is further supported by the cessation of Late Palaeozoic platform-type deposition on the passive margin of the Cimmerian block in the Central Iran during the Middle to Late Triassic (Fursich *et al*. 2005; Bagheri and Stampfli 2008) and deposition of Middle Jurassic clastic sediments in NE Iran (Zanchi *et al*. 2009). The Paleo-Tethys Ocean suture between Eurasia and the Iranian block in northern Iran is also marked by Middle to Late Palaeozoic metamorphic rocks and ophiolites that were complexly exposed in the north Iran (Figure 1).

The northward drift of the Cimmerian blocks and Iran resulted from the opening of Neo-Tethys. Most authors accept that Neo-Tethys was an immense ocean that started to open along the eastern Gondwana margin in the Late Carboniferous to Early Permian, followed by sea-floor spreading starting in the Late Early Permian associated with the drifting of the Cimmerian superterrane and the final closure of Paleo-Tethys in the Middle Triassic (e.g. Sengör 1990; Stampfli and Borel 2002; Angiolini *et al*. 2007; Golonka 2007; Zanchi *et al*. 2009; Arefifard 2017). Although Late Palaeozoic rock associations of Iran are rare, they are key to reconstructing the evolution of the Tethyan oceans (Table 1 and references therein) (Figure 1). The Late Palaeozoic A-type units are overlain by Permian to Early Mesozoic marine sediments, consistent with an extensional regime in the Late Palaeozoic. This is further substantiated by the coeval bimodal magmatism exposed in northwestern Iran (Alirezaei and Hassanzadeh 2012; Saccani *et al*. 2013; Shakerardakani *et al*. 2015; Shafaii Moghadam *et al*. 2015b; Azizi *et al*. 2017). The U-Pb ages obtained from the Late Palaeozoic A-type igneous rocks of Iran along with some mafic rocks, orthogneiss and amphibolite (Table 1 and Figure 7) indicate that the rifting of the Iranian Cimmerian terranes from northern Gondwana and the opening of the Neo-Tethys Ocean was probably initiated in the Late Devonian to Early Carboniferous at the onset of Hercynian orogeny outside of Iran. However, Delavari *et al*. (2019) controversially argued that the Pir-Eshagh acidic volcanic rocks were formed during the Hercynian orogeny in a post-collisional tectonic setting based on zircon U-Pb age of ~298 Ma obtained from an ignimbrite rhyolite sample (Table 1). At the same time, they stated that the Devonian basic volcanic rocks, exposed adjacent to the Pir-Eshagh area, imply their formation in a within-plate and non subduction environment. The age data may indicate that volcanic eruption was active during the Late Devonian to Early Permian in the Pir-Eshagh area.

The geodynamic evolution of the Neo-Tethys Ocean is now relatively well constrained. During the northward subduction of the Neo-Tethys oceanic lithosphere beneath the Iranian plate (part of the Cimmerian block) in the Mesozoic, the Sanandaj-Sirjan zone occupied the position of a magmatic arc. It is generally accepted that subduction started during the Early to Middle Jurassic, but controversy still exists regarding the Neo-Tethys closure time and continental collision between the Arabian and Iranian plates, variously proposed to have been Late Cretaceous (e.g. Berberian and King 1981; Mohajjel and Fergusson 2000; Mohajjel *et al*. 2003; Azizi and Jahangiri 2008), Eocene (e.g. Ghasemi and Talbot 2006; Mazhari *et al*. 2009), Miocene (e.g. Omrani *et al*. 2008; Azizi and Moinevaziri 2009) and or as asynchronous from north to south in Late Cretaceous to Late Palaeocene and Middle to Late Miocene receptively (Jafari *et al*. 2018).

7. Conclusions

1- The studied rhyolites have the geochemical features of the A_1 subtype of A-type magmas and provide evidence for extensional tectonics and rifting of Cimmerian fragments away from Gondwana during the Late Palaeozoic. Zircon U-Pb dating and geochemical investigations suggest that they were generated by fractional crystallization from an enriched mantle-derived mafic parental magma, with crustal interactions at 339.7 ± 2.7 Ma, during the Early Carboniferous.

2- The Late Palaeozoic rock associations of Iran define a parallel trend consistent with the Neo-Tethys suture zone. Considering the U-Pb ages obtained from those rocks it can be inferred that the opening of Neo-Tethys and continental break-up that separated Iran from Gondwana started in the Late Devonian to Early Carboniferous.

3- Reconstruction of the Tethyan oceans indicates that the Iranian micro-continents, as Cimmerian terranes, were remote from the Proto-Tethys Ocean

Acknowledgments

Most of the laboratory work was carried out at Research School of Earth Sciences, Australian National University. The first author would like to thank Prof. Trevor Ireland for providing access to the ion microprobe facilities, Prof. Vickie C. Bennett for her support with ICP-MS and Mr. Shane Paxton for his contributions and assistance with zircon separation. Invaluable comments and suggestion by Gültekin Topuz and two anonymous referees and great editorial contributions from Robert Stern are highly appreciated.

Disclosure statement

No potential conflict of interest was reported by the authors.

Research highlights

- Pir-Eshagh rhyolite exhibits the geochemical character of A_1 subtype of A-type magmas
- Petrogenesis of the Pir-Eshagh rhyolite highlights the rocks forming by the fractional crystallization from a mantle-derived mafic magma.
- Gondwana breakup through the Neotethys opening initiated in the Late Devonian to Early Carboniferous

References

Abalos, B., Carreras, J., Druguet, E., Viruete, J.E., Pugnaire, M.T.G., Alvarez, S.L., Quesada, C., Fernandez, L.R.R., and Gil-Ibarguchi, J. I., 2002, Variscan and pre-Variscan tectonics: The Geological Society of London, p. 155–183. doi:10.1144/GOSPP.9.

Advay, M., and Ghalamghash, J., 2011, Petrogenesis and U–Pb dating zircon of granites of Heris (NW of Shabestar), eastern Azerbaigan province: Iranian Journal Crystallography Mineralogy, -v. 4, p. 633–648. [(In Persian with English abstract)].

Agard, P., Omrani, J., Jolivet, L., Whitechurch, H., Vrielynck, B., Spakman, W., Monié, P., Meyer, B., and Wortel, R., 2011, Zagros orogeny: A subduction-dominated process. Geological Magazine, v. 148, p. 692–725. doi:10.1017/S001675681100046X

Aghanabati, A., 2006, Geology of Iran: Geological Survey of Iran Publications. (In Persian).

Alavi, M., 1991, Sedimentary and structural characteristics of the Paleo-Tethys remnants in northeastern Iran: Geological Society of America Bulletin, v. 103, no. 8, p. 983–992. doi:10.1130/0016-7606(1991)103<0983:SASCOT>2.3.CO;2.

Alirezaei, S., and Hassanzadeh, J., 2012, Geochemistry and zircon geochronology of the Permian A-type Hasanrobat granite, Sanandaj–Sirjan belt: A new record of the Gondwana break-up in Iran: Lithos, v. 151, p. 122–134. doi:10.1016/j.lithos.2011.11.015.

Allen, M.B., Saville, C., Blanc, E.J.P., Talebian, M., and Nissen, E., 2013, Orogenic plateau growth: Expansion of the Turkish-Iranian Plateau across the Zagros fold-and-thrust belt: Tectonics, v. 32, no. 2, p. 1–20. doi:10.1002/tect.20025.

Angiolini, L., Gaetani, M., Muttoni, G., Stephenson, M.H., and Zanchi, A., 2007, Tethyan oceanic currents and climate gradients 300 m.y. ago: Geology, v. 35, no. 12, p. 1071–1074. doi:10.1130/G24031A.1.

Arefifard, S., 2017, Foraminiferal-based paleobiogeographic reconstructions in the Carboniferous of Iran and its implications for the Neo-Tethys opening time: A synthesis: Geologica Acta, v. 15, p. 135–151. doi:10.1344/GeologicaActa2017.15.2.5.

Asadpour, M., Pourmoafi, S.M., and Heuss, S., 2013, Geochemistry, petrology and U-Pb geochronology of Ghazan mafic-ultramafic intrusion, NW Iran: Petrology, v. 4, no. 14, p. 1–16. [(in Persian with English abstract)].

Authemayou, C., Chardon, D., Bellier, O., Malekzadeh, Z., Shabanian, E., and Abbassi, M.R., 2006, Late Cenozoic partitioning of oblique plate convergence in the Zagros fold-and-thrust belt (Iran): Tectonics, v. 25, no. 3, p. TC3002. doi:10.1029/2005TC001860.

Azizi, H., and Jahangiri, A., 2008, Cretaceous subduction-related volcanism in the northern Sanandaj-Sirjan Zone, Iran: Journal of Geodynamics, v. 45, no. 4–5, p. 178–190. doi:10.1016/j.jog.2007.11.001.

Azizi, H., Kazemi, T., and Asahara, Y., 2017, A-type granitoid in Hasansalaran complex, northwestern Iran: Evidence for extensional tectonic regime in northern Gondwana in the Late Paleozoic: Journal of Geodynamics, v. 108, p. 56–72. doi:10.1016/j.jog.2017.05.003.

Azizi, H., and Moinevaziri, H., 2009, Review of the tectonic setting of Cretaceous to Quaternary volcanism in northwestern Iran: Journal of Geodynamics, v. 47, no. 4, p. 167–179. doi:10.1016/j.jog.2008.12.002.

Badr, A., Davoudian, A.R., Shabanian, N., Azizi, H., Asahara, Y., Neubauer, N., Dong, Y., and Yamamoto, K., 2018, A- and I-type metagranites from the North Shahrekord Metamorphic Complex, Iran: Evidence for Early Paleozoic post-collisional magmatism: Lithos, v. 300–301, p. 86–104. doi:10.1016/j.lithos.2017.12.008.

Bagheri, S., and Stampfli, G.M., 2008, The Anarak, Jandaq and Posht-e-Badam metamorphic complexes in central Iran: New geological data, relationships and tectonic implications: Tectonophysics, v. 451, no. 1–4, p. 123–155. doi:10.1016/j.tecto.2007.11.047.

Bea, F., Mazhari, A., Montero, P., Amini, S., and Ghalamghash, J., 2011, Zircon dating, Sr and Nd isotopes, and element geochemistry of the Khalifan pluton, NW Iran: Evidence for Variscan magmatism in a supposedly Cimmerian superterrane: Journal of Asian Earth Sciences, v. 40, no. 1, p. 172–179. doi:10.1016/j.jseaes.2010.08.005.

Berberian, M., 1995, Master blind thrust faults hidden under the Zagros folds: Active basement tectonics and surface morphotectonics: Tectonophysics, v. 241, no. 3–4, p. 193–224. doi:10.1016/0040-1951(94)00185-C.

Berberian, M., and King, G.C.P., 1981, Towards a paleogeography and tectonic evolution of Iran: Canadian Journal of Earth Sciences, v. 18, no. 2, p. 210–265. doi:10.1139/e81-019.

Black, L.P., Kamo, S.L., Allen, C.M., Davis, D.W., Aleinikoff, J.N., Valley, J.W., Mundil, R., Campbell, .I.H., Korsch, R.J., Williams, I. S., and Foudoulis, C., 2004, Improved 206Pb/238U microprobe geochronology by the monitoring of a trace-element-related matrix effect: SHRIMP, ID-TIMS, ELA-ICP-MS and oxygen isotope documentation for a series of zircon standards: Chemical Geology, v. 205, no. 1–2, p. 115–140. doi:10.1016/j.chemgeo.2004.01.003.

Bosold, A., Schwarzhans, W., Julapour, A., Ashrafzadeh, A.R., and Ehsani, S.M., 2005, The structural geology of the High Central Zagros revisited (Iran): Petroleum Science, v. 11, p. 225–238. doi:10.1144/1354-079304-646.

Chappell, B.W., and White, A.J.R., 1974, Two contrasting granite types: Pacific Geology. v. 8, p. 173–174.

Clemens, J.D., Holloway, J.R., and White, A.R.J., 1986, Origin of A-type granite: Experimental constraints: American Mineralogist, v. 79, p. 71–86. doi:10.1007/BF00374895.

Collins, W.J., Beams, S.D., White, A.J.R., and Chappell, B.W., 1982, Nature and origin of A-type granites with particular reference to southeastern Australia: Contributions to Mineralogy and Petrology, v. 80, no. 2, p. 189–200. doi:10.1007/BF00374895.

Condie, K.C., 1997, Sources of Proterozoic mafic dyke swarms: Constraints from Th/Ta and La/Yb ratios: Precambrian Research, v. 81, no. 1–2, p. 3–14. doi:10.1016/S0301-9268(96)00020-4.

Creaser, R.A., Price, R.C., and Wormold, R.J., 1991, A-type granite revised: Assessment of residual source model: Geology, v. 19, no. 2, p. 163–166. doi:10.1130/0091-7613(1991)019<0163:ATGRAO>2.3.CO;2.

Dall'Agnol, R., and de Oliveira, D.C., 2007, Oxidized, Magnetite-Series, Rapakivi-Type Granites of Carajás, Brazil: Implications for Classification and Petrogenesis of A-Type Granites: Lithos, v. 93, no. 3–4, p. 215–233. doi:10.1016/j.lithos.2006.03.065.

Delavari, M., Arab-Asadi, F., and Mohammadi, A., 2019, Paleozoic magmatism in the southwest of Julfa (northwestern Iran): Geochemical characteristics, U-Pb dating and tectonic setting: Petrology, v. 38, p. 99–120. [(in Persian with English abstract)].

Deng, C., Sun, D., Sun, G., Lv, C., Qin, Z., Ping, X., and Li, G., 2018, Age and geochemistry of Early Ordovician A-type granites in the Northeastern Songnen Block, NE China: Acta Geochimica, v. 37, no. 6, p. 805–819. doi:10.1007/s11631-018-0294-3.

Dias, R., and Ribeiro, A., 1995, The Ibero-Armorican Arc: A collision effect against an irregular continent?: Tectonophysics, v. 246, no. 1–3, p. 113–128. doi:10.1016/0040-1951(94)00253-6.

Eby, G.N., 1990, The A-type granitoids a review of their occurrence and chemical characteristics and speculations their petrogenesis: Lithos, v. 26, no. 1–2, p. 115–134. doi:10.1016/0024-4937(90)90043-Z.

Eby, G.N., 1992, Chemical subdivision of the A-type granitoids: Petrogenetic and tectonic Implications: Geology, v. 20, no. 7, p. 641–644. doi:10.1130/0091-7613(1992)020<0641:CSOTAT>2.3.CO;2.

Fitton, J.G., Saunders, A.D., Norry, M.J., Hardarson, B.S., and Taylor, R.N., 1997, Thermal and chemical Of the Iceland plume: Earth and Planetary Science Letters, v. 153, no. 3–4, p. 197–208. doi:10.1016/S0012-821X(97)00170-2.

Frost, B.R., Arculus, R.J., Barnes, C.G., Collins, W.J., Ellis, D.J., and Frost, C.D., 2001, A geochemical classification of granitic rocks: Journal of Petrology, v. 42, no. 11, p. 2033–2048. doi:10.1093/petrology/42.11.2033.

Fursich, F.T., Wilmsen, M., Seyed-Emami, K., Cecca, F., and Majidifard, R., 2005, The upper Shemshak Formation (Toarcian-Aalenian) of the Eastern Alborz (Iran): Biota and palaeoenvironments during a transgressive-regressive cycle: Facies, v. 51, no. 1–4, p. 365–384. doi:10.1007/s10347-005-0051-z.

Garzanti, E., and Sciunnach, D., 1997, Early Carboniferous onset of Gondwanian glaciation and Neo-Tethyan rifting in Southern Tibet: Earth Planetary Science Letters, v. 148, no. 1–2, p. 359–365. doi:10.1016/S0012-821X(97)00028-9.

Ghasemi, A., and Talbot, C.J., 2006, A new tectonic scenario for the Sanandaj-Sirjan Zone (Iran): Journal of Asian Earth Sciences, v. 26, no. 6, p. 683–693. doi:10.1016/j.jseaes.2005.01.003.

Ghasemi, H., Jutea, T., Bellon, H., Sabzehei, M., Whitechurch, H., and Ricou, L.E., 2002, The mafic-ultramafic complex of Sikhoran (Central Iran): A polygenetic ophiolite complex: ? Comptes Rendus Geoscience, v. 334, no. 6, p. 431–438. doi:10.1016/S1631-0713(02)01770-4.

Ghorbani, M., 2013, The Economic Geology of Iran Mineral Deposits and Natural Resources: Dordrecht, Springer Science Business Media, p. 581. doi:10.1007/978-94-007-5625-0.

Golonka, J., 2007, Phanerozoic paleoenvironment and paleolithofacies maps: Late Paleozoic: Geologia, v. 33, no. 2, p. 145–209.

Gorring, M., Singer, B., Jason, G., and Kay, S.M., 2003, Plio-Pleistocene basalts from the Meseta del Lago Buenos Aires, Argentina: Evidence for asthenosphere lithosphere interactions during slab window magmatism: Chemical Geology, v. 193, no. 3–4, p. 215–235. doi:10.1016/S0009-2541(02)00249-8.

Gosselet, J., 1879, Nouveaux documents pour l'étude du Famennien –Tranchées de chemin de fer entre Féron et Sémeries: Schistesde Sains. Annales de la Société géologique du Nord. v. 6, p. 389–399.

Gumming, G.L., and Richards, J.R., 1975, Ore lead isotope ratios in a continuously changing earth: Earth and Planetary Science Letters, v. 28, p. 155-171. doi:10.1016/0012-821X(75)90223-X.

Hajialioghli, R., Moazzen, M., Droop, G.T.R., Oberhänsli, R., Bousquet, R., Jahangiri, A., and Ziemann, M., 2007, Serpentine polymorphs and P-T evolution of metaperidotites and serpentinites in the Takab area, NW Iran: Mineralogical Magazine, v. 71, p. 203–222. doi:10.1180/minmag.2007.071.2.203.

Honarmand, M., Li, X.H., Nabataian, G., and Neubauer, F., 2017, In-situ zircon U-Pb age and Hf-O isotopic constraints on the origin of the Hasan-Robat A-typr granite from Sanandaj-Sirjan zone, Iran: Implications for reworking of Cadomain arc igneous rocks: Mineralogy and Petrology, v. 111, p. 659–675. doi:10.1007/s00710-016-0490-y.

Irvine, T.N., and Baragar, W.R.A., 1971, A guide to chemical classification of the common volcanic rocks: Canadian Journal of Earth Sciences, v. 8, p. 523–548. doi:10.1139/e71-055.

Jafari, A., Fazlnia, A.N., and Jamei, S., 2018, Geochemistry, petrology and geodynamic setting of the Urumieh plutonic complex, Sanandaj-Sirjan zone, NW Iran: New implication for Arabian and Central Iranian plate collision: Journal of African Earth Sciences, v. 139, p. 421–439. doi:10.1016/j.jafrearsci.2017.11.039.

James, G.A., and Wynd, J.G., 1965, Stratigraphic nomenclatures of Iranian oil consortium agreement area: American

Association of Petroleum Geologists Bulletin. v. 49, p. 2182–2245.
Karimpour, M.H., Farmer, L., Ashouri, C., and Saadat, S., 2006, Major, Trace and REE geochemistry of Paleo-Tethys Collision-Related Granitoids from Mashhad, Iran: Journal of Sciences, Islamic Republic of Iran, v. 17, no. 2, p. 127–145.
King, P.L., White, A.J.R., Chappell, B.W., and Allen, C.M., 1997, Characterization and origin of aluminous A-type granites from the Lachlan Fold Belt, southeastern Australia: Journal of Petrology, v. 38, p. 371–390. doi:10.1093/petroj/38.3.371.
Kolzenburg, S., Di Genova, D., Giordano, D., Hess, K.U., and Dingwell., D.B., 2018, The effect of oxygen fugacity on the rheological evolution of crystallizing basaltic melts: Earth ? and Planetary Science Letters, v. 487, p. 21–32. doi:10.1016/j.epsl.2018.01.023.
Landenberger, B., and Collins, W.J., 1996, Derivation of a-type granites from a dehydrated charnockitic lower crust: Evidence from the chaelundi complex, eastern Australia: Journal of Petrology, v. 37, p. 145–170. doi:10.1093/petrology/37.1.145.
Le Bas, M.J., Le Maitre, R.W., Streckeisen, A., and Zanettin, B., 1986, A chemical classification of volcanic rocks on the total alkali-silica diagram: Journal of Petrology, v. 27, no. 3, p. 745–750. doi:10.1093/petrology/27.3.745.
Li, S., Zhao, S., Liu, X., Cao, H., Yu, S., Li, X., Somerville, I., Yu, S., and Suo, Y., 2018, Closure of the Proto-Tethys Ocean and Early Paleozoic amalgamation of microcontinental blocks in East Asia: Earth-Science Reviews, v. 186, p. 37–75. doi:10.1016/j.earscirev.2017.01.011.
Li, X., Zhou, H., Liu, Y., Lee, C.Y., Sun, M., and Chen, C., 2000, Shoshonitic intrusive suite in SE Guangxi: Petrology and geochemistry: Chinese Science Bulletin, v. 45, p. 653–659. doi:10.1007/BF02886045.
Liu, D., Jian, P., Kroner, A., and Xu, S., 2006, Dating of prograde metamorphic events deciphered from episodic zircon growth in rocks of the Dabie–Sulu UHP complex, China: Earth and Planetary Science Letters, v. 250, p. 650–666. doi:10.1016/j.epsl.2006.07.043.
Loiselle, M.C., and Wones, D.S., 1979, Characteristics and Origin of Anorogenic Granites. Geological Society of America: Abstracts with Programs. v. 11, p. 468.
Ludwig, K.R., 2003, Isoplot 3: Berkeley, CA, Berkeley Geochronology Center, Special publication, p. 4.
Martin, R.F., 2006, A-type granites of crustal origin ultimately result from open-system fenitization-type reactions in an extensional environment: Lithos, v. 91, p. 125–136. doi:10.1016/j.lithos.2006.03.012.
Mazhari, S.A., Bea, F., Amini, S., Ghalamghash, J., Molina, J.F., Pillar, M., Scarrow, J.H., and Williams, S., 2009, The Eocene bimodal Piranshahr massif of the Sanandaj- Sirjan zone, NW Iran. A marker of the end of the collision in the Zagros Orogen: Journal of the Geological Society, v. 166, p. 53–69. doi:10.1144/0016-76492008-022.
Mbowou, G.I.B., Botelho, N.F., Lagmet, C.A., and Ngounouno, I., 2015, Petrology of peraluminous and peralkaline rhyolites from the SE Lake Chad (northernmost Cameroon Line): Journal of African Earth Sciences, v. 112, p. 129–141. doi:10.1016/j.jafrearsci.2015.09.015.
McDonough, W.F., and Sun, S.S., 1995, The Composition of the Earth: Chemical Geology, v. 120, p. 223–253. doi:10.1016/0009-2541(94)00140-4.
Moayyed, M., 2013, Petrography and Petrology of A–type rhyolites of Ghaleh–chay (Ajabshir, East-Azerbaijan): Iranian Journal of Crystallography and Mineralogy. v. 3, p. 403–416.
Mohajjel, M., and Fergusson, C.L., 2000, Dextral transpression in late-cretaceous continental collision, Sanandaj-Sirjan zone, Western Iran: Journal of Structural Geology, v. 22, no. 8, p. 1125–1139. doi:10.1016/S0191-8141(00)00023-7.
Mohajjel, M., Fergusson, C.L., and Sahandi, M.R., 2003, Cretaceous-Tertiary convergence and continental collision, Sanandaj-Sirjan zone, western Iran: Journal of Asian Earth Sciences, v. 21, no. 4, p. 397–412. doi:10.1016/S1367-9120(02)00035-4.
Mohammadi, A., Moazzen, M., Lechmann, A., and Laurent, O., 2019, Zircon U-Pb geochronology and geochemistry of Late Devonian–Carboniferous granitoids in NW Iran: Implications for the opening of Paleo-Tethys: International Geology Review, p. 1–18. doi:10.1080/00206814.2019.1675540.
Muller, D., and Groves, D.I., 1994, Potassic igneous rocks and associated gold-copper mineralization: -Lecture Notes in Earth Sciences, v. 56. p. 252. doi:10.1007/978-3-642-59665-0.
Nabavi, M.H., 1976, An Introduction to Geology of Iran: Tehran, Iran, Geological Survey of Iran publication, p. 110. [(in Persian)].
Nagudi, B., Koeberl, C., and Kurat, G., 2003, Petrography and geochemistry of the Singo granite, Uganda, and implications for its origin: Journal of African Earth Sciences, v. 36, no. 1–2, p. 73–87. doi:10.1016/S0899-5362(03)00014-9.
Omrani, J., Agard, P., Whitechurch, H., Benoit, M., Prouteau, G., and Jolivet, L., 2008, Arc magmatism and subduction history beneath the Zagros Mountains, Iran: A new report of adakites and geodynamic consequences. Lithos, v. 106, p. 380–398. doi:10.1016/j.lithos.2008.09.008
Pearce, J.A., 1983, Role of the sub-continental lithosphere in magma genesis at active continental margins, in Hawkesworth, C.J., and Norry, M.J., eds., Continental basalts and mantle xenoliths: Nantwich, Cheshire, Shiva Publications, p. 230–249.
Pearce, J.A., Harris, N.B.W., and Tindle, A.G., 1984, Trace element discrimination diagrams for the tectonic interpretation of granitic rocks: Journal of Petrology, v. 25, no. 4, p. 956–983. doi:10.1093/petrology/25.4.956.
Peccerillo, A., and Taylor, S.R., 1976, Geochemistry of Eocene calc-alkaline volcanic rocks from the Kastamonu area, Northern Turkey: Contributions to Mineralogy and Petrology, v. 58, no. 1, p. 63–81. doi:10.1007/BF00384745.
Peng, M., Wu, Y., Gao, S., Zhang, H., Wang, J., Liu, X., Gong, H., Zhou, L., Hu, Z., Liu, Y., and Yuan, H., 2012, Geochemistry, zircon U–Pb age and Hf isotope compositions of Paleoproterozoic aluminous A-type granites from the Kongling terrain, Yangtze Block: Constraints on petrogenesis and geologic implications: Gondwana Research, v. 22, no. 1, p. 140–151. doi:10.1016/j.gr.2011.08.012.
Pfänder, J.A., Münker, C., Stracke, A., and Mezger, K., 2007, Nb/Ta and Zr/Hf in ocean island basalts – Implications for crust-mantle differentiation and the fate of niobium: Earth and Planetary Science Letters, v. 254, no. 1–2, p. 158–172. doi:10.1016/j.epsl.2006.11.027.
Raimo Lahtinen, R., Huhma, H., Lahaye, Y., Lode, S., Heinonen, S., Sayab, M., and Whitehouse, M.J., 2016, Paleoproterozoic magmatism across the Archean-Proterozoic boundry in central Fennoscandia: Geochronology, geochemistry and isotopic data (Sm-Nd,

Lu-Hf, O): Lithos, v. 262, p. 507–525. doi:10.1016/j.lithos.2016.07.014.
Rapp, R.P., and Watson, E.B., 1995, Dehydration melting of metabasalt at 8-32 kbar: Implications for continental growth and crust-mantle recycling: Journal of Petrology, v. 36, no. 4, p. 891–931. doi:10.1093/petrology/36.4.891.
Robert, A.M.M., Letouzey, J., Kavoosi, M.A., Sherkati, S., Müller, C., Vergés, J., and Aghababaei, A., 2014, Structural evolution of the Kopeh Dagh fold-and-thrust belt (NE Iran) and interactions with the South Caspian Sea Basin and Amu Darya Basin: Marine and Petroleum ?geology, v. 57, p. 68–87. doi:10.1016/j.marpetgeo.2014.05.002.
Rollinson, H., 1993, Using Geochemical Data: Evaluation, Presentation, Interpretation: Harlow, England, Addison-Wesley/Longman, p. 352.
Saccani, E., Azimzadeh, Z., Dilek, Y., and Jahangiri, A., 2013, Geochronology and petrology of the Early Carboniferous Misho Mafic Complex (NW Iran), and implications for the melt evolution of Paleo-Tethyan rifting in Western Cimmeria: Lithos, v. 162, p. 264–278. doi:10.1016/j.lithos.2013.01.008.
Saki, A., 2010, Proto-Tethyan remnants in northwest Iran: Geochemistry of the gneisses and metapelitic rocks: Gondwana Research, v. 17, no. 4, p. 704–714. doi:10.1016/j.gr.2009.08.008.
Schulmann, K., Catalán, J.R.M., Lardeaux, J.M., Janousek, V., and Oggiano, G., 2014, The Variscan orogeny: Extent, timescale and the formation of the European crust: Geological Society, London, Special Publications, v. 405, no. 1, p. 1–6. doi:10.1144/SP405.15.
Sengör, A.M.C., 1989, The Tethyside orogenic system: An introduction, *in* Şengör, A.M.C., ed., Tectonic Evolution of the Tethyan Region: -Springer, Dordrecht, v. 259, p. 1–22, doi:10.1007/978-94-009-2253-2_1.
Sengör, A.M.C., 1990, A new model for the late Paleozoic-Mesozoic tectonic evolution of Iran and implications for Oman, *in* Robertson, A.H., Searle, M.P., and Ries, A.C., eds., The Geology and tectonics of the Oman region: Geological Society Special Publication, London, v. 49, p. 797–831. doi:10.1144/GSL.SP.1992.049.01.49.
Shafaii Moghadam, H., Li, X.H., Ling, X.X., Stern, R.J., Khedr, M.Z., Chiaradia, M., Ghorbani, G., Arai, S., and Tamura, A., 2015a, Devonian to Permian evolution of the Paleo-Tethys Ocean: New evidence from U-Pb zircon dating and Sr-Nd-Pb isotopes of the Darrehanjir-Mashhad ophiolites, NE Iran: Gondwana Research, v. 28, no. 2, p. 781–799. doi:10.1016/j.gr.2014.06.009.
Shafaii Moghadam, H., Li, X.H., Ling, X.X., Stern, R.J., Santos, J.F., Meinhold, G., Ghorbani, G., and Shahabi, H., 2015b, Petrogenesis and tectonic implications of Late Carboniferous A-type granites and gabbronorites in NW Iran: Geochronological and geochemical constraints: Lithos, v. 212–215, p. 266–279. doi:10.1016/j.lithos.2014.11.009.
Shafaii Moghadam, H., and Stern, J.R., 2014, Ophiolites of Iran: Keys to understanding the tectonic evolution of SW Asia: (I) Paleozoic ophiolites: Journal of Asian Earth Sciences, v. 91, p. 19–38. doi:10.1016/j.jseaes.2014.04.008.
Shafaii Moghadam, H., and Stern, J.R., 2015, Ophiolites of Iran: Keys to understanding the tectonic evolution of SW Asia: (II) Mesozoic ophiolites: Journal of Asian Earth Sciences, v. 100, p. 31–59. doi:10.1016/j.jseaes.2014.12.016.
Shahzeidi, M., Moayyed, M., Murata, M., Yui, T.F., Arai, S., Chen, F., Pirnia, T., and Ahmadian, J., 2017, Late Ediacaran crustal thickening in Iran: Geochemical and isotopic constraints from the ~550 Ma Mishu granitoids (Northwest Iran): International Geology Review, v. 59, p. 793–811. doi:10.1080/00206814.2016.1198728.
Shakerardakani, F., Neubauer, F., Masoudi, F., Mehrabi, B., Liu, X., Dong, Y., Mohajjel, M., Monfaredi, .B., and Friedl, .G., 2015, Panafrican basement and Mesozoic gabbro in the Zagros orogenic belt in the Dorud–Azna region (NW Iran): Laser-ablation ICP–MS zircon ages and geochemistry: Tectonophysics, v. 647, p. 146–171. doi:10.1016/j.tecto.2015.02.020.
Shumei, X., Huaiwei, F., Sanzhong, L., Meng, L., Somerville, I., Haiming, B., Yang, J., and Qing, Y., 2015, Closure time in the East Qilian Ocean and Early Paleozoic ocean–continent configuration in the Helan Mountains and adjacent regions, NW China: Journal of Asian Earth Sciences, v. 113, p. 575–588. doi:10.1016/j.jseaes.2015.07.031.
Soffel, H.C., and Forster, H.G., 1980, Apparent Polar Wander Path of Central Iran and its Geotectonic Interpretation: Advances in Earth and Planetary Sciences, v. 10, p. 117–135. doi:10.5636/jgg.32.Supplement3_SIII117.
Song, S., Bi, H., Qi, S., Yang, L., Allen, M.B., Niu, Y., Su, L., and Li, W., 2018, HP–UHP Metamorphic Belt in the East Kunlun Orogen: Final Closure of the Proto-Tethys Ocean and Formation of the Pan-North-China Continent: Journal of Petrology, v. 59, p. 2043–2060. doi:10.1093/petrology/egy089.
Stampfli, G.M., 2000, Tethyan oceans: Geological Society, London, Special Publications, v. 173, no. 1, p. 1–23. doi:10.1144/GSL.SP.2000.173.01.01.
Stampfli, G.M., and Borel, G.D., 2002, A plate tectonic model for the Paleozoic and Mesozoic constrained by dynamic plate boundaries and restored synthetic oceanic isochrones: Earth and Planetary Science Letters, v. 196, no. 1–2, p. 17–33. doi:10.1016/S0012-821X(01)00588-X.
Stampfli, G.M., and Kozur, H., 2006, Europe from the Variscan to the Alpine cycles, *in* Gee, D.G., and Stephenson, R., eds., European Lithosphere Dynamics: London, Memoir of the Geological Society, p. 57–82. doi:10.1144/GSL.MEM.2006.032.01.04.
Stampfli, G.M., Mosar, J., Favre, P., Pillevuit, A., and Vanney, J.C., 2001, Permo Mesozoic Evolution of the Western Tethys Realm: The Neotethys East Mediterranean Basin connection: Memoires Du Museum National D Historie Naturelle. v. 186, p. 51–108.
Sun, S.S., and McDonough, W.F., 1989, Chemical and isotopic systematics of oceanic basalts: Implications for mantle composition and processes: Geological Society, London, Special Publications, v. 42, no. 1, p. 313–345. doi:10.1144/GSL.SP.1989.042.01.19.
Taylor, S.R., and McLennan, S.M., 1985, The continental crust: Its composition and evolution: Blackwell Scientific Publications, Oxford, p. 1–312.
Topuz, G., Hegner, E., Homam, S.M., Ackerman, L., Pfänder, J.A., and Karimi, H., 2018, Geochemical and geochronological evidence for a Middle Permian oceanic plateau fragment in the Paleo-Tethyan suture zone of NE Iran: Contributions to Mineralogy and Petrology, v. 173, no. 10, p. 81. doi:-doi:10.1007/s00410-018-1506-x.

Torsvik, T.H., and Cocks, L.R.M., 2004, Earth geography from 400 to 250 Ma: A paleomagnetic, faunal and facies review: Journal of the Geological Society of London, v. 161, p. 555–572. doi:10.1144/0016-764903-098.

Vander-Auwera, J., Martin, H., and Ramo, T., 2003, Origin and evolution of Precambrian anorogenic magmatism: Precambrian Research, v. 124, p. 105–344. doi:10.1016/S0301-9268(03)00083-4.

von Raumer, J.F., Bussy, F., Schaltegger, U., Schaltegger, U., Schulz, B., and Stampfli, G.M., 2013, Pre-Mesozoic Alpine basements — Their place in the European Paleozoic framework: Geological Society of America Bulletin, v. 125, p. 89–108. doi:10.1130/B30654.1.

von Raumer, J.F., and Stampfli, G.M., 2008, The birth of the Rheic Ocean – Early Palaeozoic subsidence patterns and subsequent tectonic plate scenarios: Tectonophysics, v. 461, p. 9–20. doi:10.1016/j.tecto.2008.04.012.

von Raumer, J.F., Stampfli, G.M., and Bussy, F., 2003, Gondwana-derived microcontinents — The constituents of the Variscan and Alpine collisional orogens: Tectonophysics, v. 365, no. 1–4, p. 7–22. doi:10.1016/S0040-1951(03)00015-5.

Weil, A.B., Van der Voo, R., and van der Pluijm, B.A., 2001, Oroclinal bending and evidence against the Pangea megashear: The Cantabria-Asturias arc (northern Spain): Geology, v. 29, no. 11, p. 991–994. doi:10.1130/0091-7613(2001)029<0991:OBAEAT>2.0.CO;2.

Whalen, J.B., Currie, K.L., and Chappel, B.W., 1987, A-type granites: Geochemical characteristics, discrimination and petrogenesis: Contributions to Mineralogy and Petrology, v. 95, no. 4, p. 407–419. doi:10.1007/BF00402202.

Whalen, J.B., Jenner, G.A., Longstaff, F.J., Robert, F., and Galiepy, C., 1996, Geochemical and isotopic (O, Nd, Pb and Sr) constraints on A-type granite petrogenesis based on the Topsails igneous suite, Newfoundland Appalachians: Journal of Petrology, v. 31, p. 1463–1489. doi:10.1093/petrology/37.6.1463.

Williams, I.S., 1998, U-Th-Pb geochronology by ion microprobe (book chapter): Reviews of Economic ?geology, v. 7, p. 1–35. doi:10.5382/Rev.07.01.

Wilmsen, M., Fursich, T., Emami, K.S., Majidifard, M.R., and Taheri, M.R., 2009, The Cimmerian Orogeny in northern Iran: Tectono-stratigraphic evidence from the foreland: Terra Nova, v. 21, p. 221–318. doi:10.1111/j.1365-3121.2009.00876.x.

Zanchetta, S., Berra, F., Zanchi, A., Bergomi, M., Caridroit, M., Nicora, A., and Heidarzadeh, G., 2013, The record of the Late Paleozoic active margin of the Palaeotethys in NE Iran: Constraints on the Cimmerian orogeny: Gondwana Research, v. 24, p. 1237–1266. doi:10.1016/j.gr.2013.02.013.

Zanchi, A., Zanchetta, S., Berra, F., Mattei, M., Garzanti, E., Molyneux, S., Nawab, A., and Sabouri, J., 2009, The Eo-Cimmerian (Late? Triassic) orogeny in North Iran: GSL Special Publications, v. 312, p. 31–56. doi:10.1144/SP312.3.

Zhang, Z.M., Dong, X., Liu, F., Lin, Y.H., Yan, R., He, Z.Y., and Santosh, M., 2012, The making of Gondwana: Discovery of 650 Ma HP granulites from the North Lhasa, Tibet: Precambrian Research, v. 213, p. 212–213. doi:10.1016/j.precamres.2012.04.018.

Zhao, G., Wang, Y., Huang, B., Dong, Y., Li, S., Zhang, G., and Yu, S., 2018, Geological reconstructions of the East Asian blocks: From the breakup of Rodinia to the assembly of Pangea: Earth-Science Reviews, v. 186, p. 262–286. doi:10.1016/j.earscirev.2018.10.003.

Ziegler, A.M., Scotese, C.R., Mckerroww, S., Johnson, M.E., and Bambach, R.K., 1979, Paleozoic paleogeography: Annual Review of Earth and Planetary Sciences, v. 7, no. 1, p. 473–502. doi:10.1146/annurev.ea.07.050179.002353.

Ziegler, P.A., Cloetingh, S., Guiraud, R., and Stampfli, G.M., 2001, Peri-Tethyan platforms: Constraints on dynamics of rifiting and basin inversion: Memoires du Muséum National d'Historie Naturelle, Paris, Peri-Tethys Memoir. v. 6, p. 9–49.